Published online 29 April 2017

Nucleic Acids Research, 2017, Vol. 45, No. 10 ***5945–5957***
doi: 10.1093/nar/gkx326

Proteomic analysis of polyribosomes identifies splicing factors as potential regulators of translation during mitosis

Ranen Aviner[1,*,†], Sarah Hofmann[1,†], Tamar Elman[1], Anjana Shenoy[2], Tamar Geiger[2], Ran Elkon[2], Marcelo Ehrlich[1] and Orna Elroy-Stein[1,*]

[1]Department of Cell Research & Immunology, George S. Wise Faculty of Life Sciences, Tel Aviv University, Tel Aviv 69978, Israel and [2]Department of Human Molecular Genetics and Biochemistry, Sackler Faculty of Medicine, Tel Aviv University, Tel Aviv 69978, Israel

Received January 26, 2017; Revised April 10, 2017; Editorial Decision April 13, 2017; Accepted April 16, 2017

ABSTRACT

Precise regulation of mRNA translation is critical for proper cell division, but little is known about the factors that mediate it. To identify mRNA-binding proteins that regulate translation during mitosis, we analyzed the composition of polysomes from interphase and mitotic cells using unbiased quantitative mass-spectrometry (LC–MS/MS). We found that mitotic polysomes are enriched with a subset of proteins involved in RNA processing, including alternative splicing and RNA export. To demonstrate that these may indeed be regulators of translation, we focused on heterogeneous nuclear ribonucleoprotein C (hnRNP C) as a test case and confirmed that it is recruited to elongating ribosomes during mitosis. Then, using a combination of pulsed SILAC, metabolic labeling and ribosome profiling, we showed that knockdown of hnRNP C affects both global and transcript-specific translation rates and found that hnRNP C is specifically important for translation of mRNAs that encode ribosomal proteins and translation factors. Taken together, our results demonstrate how proteomic analysis of polysomes can provide insight into translation regulation under various cellular conditions of interest and suggest that hnRNP C facilitates production of translation machinery components during mitosis to provide daughter cells with the ability to efficiently synthesize proteins as they enter G1 phase.

INTRODUCTION

The eukaryotic cell cycle is a tightly controlled process governed by the precisely timed expression, activation and degradation of proteins that mediate progression through the different phases. During mitosis, global translation is suppressed by phosphorylation and disruption of protein complexes required for both initiation and elongation, including eIF4F, eIF2-GTP-tRNAi^{Met}, eEF1 and eEF2 (1–4). This results in attenuation of 40S subunit recruitment as well as hindered delivery of amino acids to initiating and elongating ribosomes, leading to retention of mRNA transcripts on heavy mitotic polysomes despite the global reduction in translation rates. Retained transcripts are thus protected from degradation and available for immediate resumption of translation upon exit from mitosis (3,4). Nevertheless, ribosome profiling and mass-spectrometric (MS) analyses have identified several hundreds of mRNAs whose translation is specifically up- or down-regulated during mitosis (5–7). While some of these transcripts contain known internal ribosome entry sites (IRES) that promote an alternative cap-independent mode of initiation, many others do not, suggesting the existence of yet unknown mechanisms that may facilitate initiation and elongation on specific mRNAs despite the global attenuation of translation.

One attractive hypothesis that can explain transcript-specific translational control is the differential association of mRNA-binding proteins, many of which have been shown to selectively promote or inhibit translation of specific target mRNAs. Such proteins may bind during transcription, splicing or mRNA maturation to form messenger ribonucleoprotein (mRNP) complexes that regulate multiple aspects of mRNA metabolism and function, including localization, translation and degradation. Computational predictions and experimental work have indicated that the mammalian genome encodes up to about 1500

*To whom correspondence should be addressed. Tel: +972 3 640 9153; Fax: +972 3 642 2046; Email: OrnaES@tauex.tau.ac.il
Correspondence may also be addressed to Ranen Aviner. Email: ranen.aviner@ucsf.edu
†These authors contributed equally to this work as first author.

© The Author(s) 2017. Published by Oxford University Press on behalf of Nucleic Acids Research.
This is an Open Access article distributed under the terms of the Creative Commons Attribution License (http://creativecommons.org/licenses/by-nc/4.0/), which permits non-commercial re-use, distribution, and reproduction in any medium, provided the original work is properly cited. For commercial re-use, please contact journals.permissions@oup.com

RNA-binding proteins (8), the role of many is still unknown (reviewed in (9,10)).

To better characterize the dynamic changes in mRNA-binding proteins that interact with polysome-associated mRNAs during cell division, we analyzed polysomal complexes from interphase and mitotic cells using a quantitative proteomics approach. We found that mitotic polysomes are enriched with proteins involved in RNA processing, including alternative splicing and export factors. Focusing on heterogeneous nuclear ribonucleoprotein C (hnRNP C) as a test case for validation, we demonstrated that it associates with elongating ribosomes during mitosis to specifically promote the translation of mRNAs encoding ribosomal proteins and translation factors.

MATERIALS AND METHODS

Cell culture and synchronization

HeLa S3 cells or their derived stable shRNA expressing cell lines were cultured in DMEM supplemented with 10% fetal calf serum, 2 mM L-glutamine and 100 U/ml penicillin/streptomycin (all Biological Industries) at 37°C in 5% CO_2. For synchronization, cells were treated with 2 mM thymidine (Sigma) for 18 h, released from the G1/S block into fresh supplemented DMEM for 8 h and then treated again with 2 mM thymidine for 18 h. After release from the second block, cells were cultured for either 8.5 or 12 h before being harvested in M or G1, respectively. The efficiency of cell synchronization by double thymidine block was assessed by flow cytometry analysis following propidium iodide (Sigma) staining.

Generation of stable cell lines and induction of hnRNP C knockdown

HeLa S3 cells stably expressing Doxycycline (Dox)-inducible shRNA against hnRNP C (termed sh-hnRNP C) or scrambled shRNA (termed sh-Scramble) were generated using the Inducible TRIPZ Lentiviral shRNA system (shRNA hnRNP C: Clone ID: V3THS_401793 (Thermo Scientific); scramble shRNA: #RHS4743 (Dharmacon). To induce sh-RNA expression, cells were grown in DMEM supplemented with 0.5 μg/ml Dox (Sigma) for 72 h. Dox was added freshly to the cells every 24 h. Where indicated, synchronization by double-thymidine block was followed for 2 days in the presence of 0.5 μg/ml Dox. Knockdown efficiency was evaluated by immunoblotting of three biological replicates.

SILAC labeling and sample preparation for MS analysis

To identify proteins that are differentially associated with polysomes during mitosis, the entire proteome of HeLa S3 cells was fully labelled by culturing for 10 days in DMEM depleted of the natural amino acids lysine and arginine and supplemented with light (Lys0 and Arg0) or heavy (Lys8 and Arg10) versions of these amino acids (referred to as Light or Heavy SILAC medium, respectively). Labeled cells were then synchronized by double-thymidine block, harvested at M or G1 and subjected to polysome profiling. Proteins were extracted from the pooled polysomal fractions using methanol-chloroform, resuspended in Urea Buffer (6 M urea/2 M thiourea in 100 mM Tris–HCl (pH 8.5)) and concentrations were determined using the Bradford Protein assay (Bio-Rad). Equal protein amounts from M and G1 samples were combined prior to further processing. Two replicates consisted of light-labeled M cells and heavy-labeled G1 cells, and a third replicate consisted of heavy-labeled M cells and light-labeled G1 cells (label swap).

For the pulsed SILAC (pSILAC) experiments, sh-hnRNP C and sh-Scramble HeLa cells were first cultured for 10 days in Light SILAC medium to achieve complete labeling of the steady-state proteome. Labeled cells were further cultured for 72 h in the presence or absence of Dox in Light SILAC medium, to induce expression of shRNA. Then, cells were switched to Heavy SILAC medium for 12 additional hours in the presence or absence of Dox, harvested in PBS and lysed in Urea Buffer at RT. The experiment was performed in triplicates.

Equal amounts of protein (20 μg) from each sample were reduced with 1 mM dithiothreitol (DTT) and alkylated with 5 mM iodoacetamide (IAA). Protein digestion was performed for 3 h with endoprotease LysC (Wako chemicals; 1:100 enzyme to protein ratio) followed by an overnight digestion with sequencing grade modified Trypsin (Promega; 1:50 enzyme to protein ratio) at RT. Peptides were acidified with trifluoroacetic acid (TFA) and purified on C18 stageTips (11). Eluted peptides were separated using EASY-nLC-1000 HPLC system (Thermo Scientific) coupled to the Q Exactive Plus MS (Thermo Scientific). MS analysis was performed in a data dependent mode using a top 10 method for MS/MS acquisition.

MS data analysis

Analysis was performed with the Maxquant Software (12) (version 1.5.0.36) and MS/MS spectra were searched against the Uniprot database (May 2013) with the Andromeda search engine (13). FDR was set to 1% at both the peptide and protein levels. Multiplicity was set to two with light and heavy peptides specified and minimum ratio count for quantification was set as two. Cysteine carbamidomethylation was used as a fixed modification while methionine oxidation and protein N-terminal acetylation were set as variable modifications. Minimum peptide length allowed was six amino acids and the maximum number of missed cleavages was set to two. Raw intensities were normalized using intensity-based absolute quantification (iBAQ) (14). All subsequent data analyses were performed by Perseus (version 1.5.0.19). The data was filtered to remove reverse identified, only identified by site and potential contaminants. Volcano plots were generated using a two-tailed Student's *t*-test with FDR = 0.05, S = 0.1. ANOVA test was performed on grouped replicates with FDR = 0.01 and S0 = 0. Hierarchical clustering of proteins was performed after *z*-score normalization of the data, using Euclidean distances. The MS proteomics data are available from the ProteomeXchange Consortium via the PRIDE partner repository with the dataset identifier PXD004244. For whole cell protein abundance measurements at M or G1, we used a previously-published dataset generated from matching samples using the same procedure (15).

Polysome profiling on sucrose gradients

Frozen cell pellets from synchronized cells were thawed on ice and lysed for 10 min on ice in *polysome lysis buffer* (18 mM Tris pH 7.5, 50 mM KCl, 10 mM $MgCl_2$, 1.25 mM DTT (Sigma), 1% Triton X-100, 2 μg/ml Leupeptin (Sigma), 1.4 μg/ml Pepstatin (Roche), 1% sodium deoxycholate (Sigma), 1× complete EDTA-free protease inhibitor (Roche), and 80 U/ml RiboLock RNase inhibitor (Thermo Scientific)) supplemented with 100 μg/ml cycloheximide (Sigma). Nuclei were pelleted by centrifugation at 20 000 × g for 5 min at 4°C, and equal amounts of OD units (254 nm) from the cytoplasmic supernatant were loaded onto 10–50% sucrose gradients. Following ultracentrifugation at 34 000 rpm for 90 min at 4°C in an SW41 Beckman Coulter rotor, the gradients were fractionated using a Teledyne ISCO UA-6 UV/VIS gradient elution and detection system. Polysome profiles were obtained through continuous OD measurement at 254 nm and 18 fractions (0.6 ml each) representing the entire gradient were collected. Protein was extracted from sucrose gradient fractions by incubation with Strataclean Resin (Agilent) overnight at 4°C, followed by centrifugation at 850 × g for 5 min at 4°C, aspiration of supernatant and resuspension in 2× Laemmli buffer (0.16 M Tris–HCl, 20% glycerol, 4% SDS, 0.2 M DTT, Bromophenol blue).

Ribosome pelleting on sucrose cushion

HeLa S3 cells were synchronized into G1 and M using double-thymidine block, washed and harvested in PBS, and pellets were frozen at –80°C for subsequent use. Prior to lysis, pellets were thawed on ice and the cells were lysed for 20 min in *polysome lysis* buffer (see above). The lysate was cleared by centrifugation at 20 000 x g for 10 min at 4°C, and the supernatant was layered onto 500 μl of a 2 M sucrose cushion, following ultracentrifugation at 37 000 rpm for 4 h at 4°C in a Beckman Coulter TLA120.2 rotor. The ribosome pellet was resuspended in *polysome lysis* buffer and further analyzed by immunoblot analysis.

Immunoblot analysis

Proteins from whole cell extracts or sucrose gradient fractions were separated by 10 or 12% SDS-PAGE followed by Western immunoblot analysis using the following antibodies: mouse anti-hnRNP C1/C2 (clone 4F4, Millipore 05-1520, 1:500), rabbit anti-PABP (clone H-300, Santa Cruz Biotechnology sc-28834, 1:3000), rabbit anti-RPL26 (Abcam ab59567, 1:3000), RPLP0 (Abcam ab101279, 1:2000), anti-Sm (Y12), which also cross-reacts with RPS10 (16) (gift from Dr Joseph Sperling, 1:1000), rabbit anti-ERH (Santa Cruz Biotechnology sc-96130, 1:1000), mouse anti-SRSF10 (Santa Cruz Biotechnology sc-77209, 1:1000), rabbit anti-hnRNP G/RBMX (Santa Cruz Biotechnology sc-48796, 1:500), mouse anti-eIF4A3 (clone B2, Santa Cruz Biotechnology sc-365549, 1:1000), rabbit anti-Tra2B (Santa Cruz Biotechnology sc-31353, 1:1000), mouse anti-hnRNP F/H (Santa Cruz Biotechnology sc-32310, 1:1000), rabbit anti-SF2/SRSF1 (Santa Cruz Biotechnology sc-38017, 1:1000), rabbit anti-beta-tubulin (clone 9F3, Cell Signaling Technology #2128, 1:10 000), mouse anti-Cyclin B1 (Abcam ab72, 1:1000), mouse anti-puromycin antibody (clone 12D10, Millipore MABE343, 1:1000). Secondary antibodies: HRP-conjugated anti-rabbit IgG, HRP-conjugated anti-mouse IgG, (Jackson ImmunoResearch Laboratories, 1:10 000).

Immunohistochemistry and quantitative image analysis

U2OS cells expressing RFP-tagged Lamin A (17) or HeLa S3 cells seeded at 5 × 10^4 cells/well on coverslips in 24-well plates were fixed at 24 h by incubation with 4% paraformaldehyde for 10 min at room temperature (RT) and then blocked for 1 h with phosphate-buffered saline (PBS) supplemented with 5% normal goat serum and 0.1% Triton X-100. The coverslips were then incubated for 1 h in PBS containing 4% bovine serum albumin (BSA) and rabbit anti-RPS6 (Cell Signaling 2217, 1:250) together with either mouse anti-hnRNP C1/C2 (clone 4F4, Millipore 05-1520, 1:1000) or mouse anti-hnRNP F/H (Santa Cruz Biotechnology sc-32310, 1:1000). Following three washes with PBS, the coverslips were incubated for 2 h at RT with PBS containing 4% BSA, AlexaFluor-647 Donkey anti-rabbit IgG (Invitrogen A-31573, 1:2000), AlexaFlour-488 Donkey anti-mouse IgG (Abcam ab150109, 1:2500) and 2 μg/ml Hoechst (Thermo Scientific 33342). Following three washes with PBS, the coverslips were mounted onto glass slides using vinol (14% polyvinol-alcohol (Sigma P8136), 30% glycerol, in PBS). For quantitative image analysis, cells were imaged by spinning disk confocal microscopy. The microscopy setup included a CSU-22 Confocal, Yokogawa; Head; Axiovert 200M, Zeiss microscope, CW diode-pumped 473, 561 and 660 nm lasers, Plan-Fluar 100× NA 1.45 lens, Zeiss; Cobolt; Evolve camera, Photometrics; all under the control of SlideBook™ Intelligent Imaging Innovations. Cell volumes were imaged with a step size of 0.2 μm. Image rendering was with SlideBook™. To visualize differences in the spatial distribution of the fluorescence staining of hnRNP C in different cells, we selected a single midplane and rendered it with the 'pseudocolor' function of SlideBook™. In order to compare images, similar normalization settings were employed, where 70% of maximum intensity was set as full saturation.

Immunoprecipitation of hnRNP C-ribosome complexes followed by puromycin labeling

HeLa S3 cells were synchronized to mitosis and ribosomes were extracted by ultracentrifugation through a sucrose cushion (see above). The pellets were resuspended in *polysome lysis* buffer (see above) without sodium deoxycholate and incubated with 10 μg mouse anti-hnRNP C1/C2 antibodies (clone 4F4, Millipore 05-1520) or IgG control (Millipore) at 4°C for 2 h with constant rotation. 100 μl of protein G sepharose slurry (GE Healthcare) were washed twice with *polysome lysis* buffer without sodium deoxycholate and incubated with the sample-antibody mix at 4°C for 1 h with constant rotation. The beads were washed seven times with *polysome lysis* without sodium deoxycholate and incubated with 1 nM biotin-puromycin (Dharmacon) at 37°C for 15 min, to label nascent polypeptide chains. The reaction was terminated by adding Laemmli sample buffer and heating to 95°C for 5 min.

Puromycin labeling of newly-synthesized proteins in cultured cells and their detection

HeLa S3 cells were grown in supplemented DMEM and treated with Dox for 72 h to induce shRNA expression. Newly-synthesized proteins were labeled by treatment with 1 μM puromycin (Calbiochem) for 5 min. Cells were washed with PBS and harvested in 2× Laemmli sample buffer, followed by boiling at 95°C for 5 min. Samples were loaded on a 10% SDS-PAGE, transferred to a nitrocellulose membrane and immunoblotted with anti-puromycin antibody (clone 12D10, Millipore MABE343).

Extraction of RNA from sucrose gradients and qPCR

Fifteen fractions (0.7 ml each) representing the entire sucrose gradient were collected individually in tubes containing 60 μl of 10% SDS and immediately frozen at –20°C. Prior to the extraction, the samples were thawed on ice and then mixed with one volume of a phenol:chloroform:isoamyl mixture (RiboEx, GeneAll) followed by 5 min incubation at RT. After centrifugation at 12 000 × g for 15 min at 4°C, the aqueous phase from each tube was mixed with equal volume of isopropanol for RNA precipitation overnight at –20°C. 1 μg of RNA from each fraction was then used for cDNA synthesis using the qScript™ cDNA Synthesis Kit (Quanta Biosciences) according to the manufacturer's instructions. Real time quantitative PCR (qPCR) was performed using PerfeCTa SYBR Green FastMix, ROX (Quanta Biosciences) with final concentration of 300 nM for each oligonucleotide primer in a final volume of 20 μl. Primer sequences and their respective targets are listed below. Target mRNA amount in each fraction was normalized to GAPDH mRNA level followed by calculation of relative quantification (RQ) values as $RQ = 2^{-\Delta\Delta Ct}$, where ΔΔCt is the normalized cycle threshold (Ct) value in each fraction calibrated to the last fraction of each gradient. Standard deviations were calculated from three individual experiments. The following oligonucleotides were used as primers: GAPDH FWD: 5′-GCACCGTCAAGG CTGAGAAC-3′, GAPDH REV: 5′-ATGGTGGTGAAG ACGCCAGT-3′, HNRNP C1/2 FWD: 5′-CCTCGAAA CGTCAGCGTGTA-3′, HNRNP C1/2 REV: 5′-CAGA CTTGGAAGATCCCCGC-3′, RPL12 FWD: 5′-AGAA CAGACAGGCCCAGATTG-3′, RPL12 REV: 5′-GTGG TTCCTTGAGGGCTTTG-3′, RPL34 FWD: 5′-TGTCCC GAACCCCTGGTAAT-3′, RPL34 REV: 5′-GTCTTACA GCACGAACCCCT-3′, RPS9 FWD: 5′-GTGGTTTGCT TAGGCGCAG-3′, RPS9 REV: 5′-TTCAGCTCTTGGTC GAGACG-3′, RPS18 FWD: 5′-CACGCCAGTACAAG ATCCCA-3′, RPS18 REV: 5′-TTCACGGAGCTTGTTG TCCA-3′, CCNB1 FWD: 5′-GCACCAAATCAGACAG ATGG-3′, CCNB1 REV: 5′-CGACATCAACCTCTCCAA TC-3′, CCNA2 FWD: 5′-TAGATGCTGACCCATACC TC-3′, CCNA2 REV: 5′-GATTCAGGCCAGCTTTGT C-3′, TOP2B FWD: 5′-GGTACTGGATGGGCTTGTA-3′, TOP2B REV: 5′-GTTTGGAAGCATGGGATGAG-3′, PKM FWD: 5′-CATTCATCCGCAAGGCATC-3′, PKM REV: 5′-TCATCAAACCTCCGAACCC-3′.

Ribo-seq and total RNA-seq

Knockdown of hnRNP C by Dox treatment was induced in HeLa S3 cells for 3 days, followed by synchronization into M-phase by double-thymidine block for two additional days in the presence of Dox. Ribosome profiling was performed as described previously (18). Briefly, cells were lysed in lysis buffer containing 20 mM Tris pH 7.4, 150 mM NaCl, 5 mM $MgCl_2$, 1 mM DTT, 100 μg/ml Cycloheximide, 1% Triton X-100 and 25 U/ml DNase I (Ambion). The samples were treated with RNase I (Ambion) to generate ribosome footprints, and an undigested portion was used to isolate total mRNA using poly-dT agarose (Ambion). rRNA depletion was achieved using Ribo-Zero (Epicentre). The footprint fragments of size between 26 and 34 nt were separated by gel electrophoresis followed by their purification from the gel. For total RNA analysis, the purified poly-A RNA was heat-fragmented followed by separation by gel electrophoresis and purification of fragments of size between 100 and 200 nt from the gel. Linker ligation was done using the Universal miRNA cloning linker and T4 RNA ligase 2 (both from New England Biolabs). The Sequencing library was generated following reverse transcription and PCR amplification with barcoded primers using KAPA HiFi polymerase (KAPA Biosystems). Sequencing was done using Illumina HiSeq 2500 fifty base pairs single read. Libraries were generated from two biological replicates. Sequenced reads were aligned to a reference set of human curated protein-coding transcripts (plus the five human rRNA transcripts) using bowtie2 (19). This reference set of transcripts was based on Ensembl gene annotations (release 65). Alignment statistics are provided in Supplementary Table S1. For genes with multiple isoforms, the one with longest coding DNA sequence (CDS) region (and in case not unique, the one with longest UTRs among the ones with the longest CDS) was selected to represent the gene. Only uniquely mapped reads were used in subsequent analyses. RNA expression levels and ribosome occupancy were estimated by calculating reads per kilobase of mRNA per million reads (RPKM) per transcript, taking into account either all reads that map to the transcript (for estimation of RNA levels using RNA-seq data) or only those mapping to its CDS (for estimation of ribosome occupancy). In estimation of ribosome occupancy in CDS, 5′ ends of reads were offset 12 nucleotides to the 3′ direction to match the P-site location of ribosome (20). Expression estimates were further normalized using quantile normalization (21). RNA-seq and Ribo-seq datasets were combined according to gene ID. Only genes with expression level of at least 1.0 RPKM, in either the treated or control conditions, in both the RNA-seq and Ribo-seq datasets were included in subsequent analyses. The combined dataset includes 10 996 genes. Fold change (FC) in mRNA level and ribosome occupancy upon Dox treatment were calculated per gene (in $\log_2$). To avoid inflation of FC estimates due to low levels, RPKM levels below 1.0 were set to a floor level of 1.0. Translational efficiency (TE) was estimated for each gene by the ($\log_2$) ratio between its ribosome occupancy and mRNA levels. For alternative splicing analysis, reads were aligned to the human genome using TopHat2 (22) and AS events were

detected using DEXSeq (23). All sequence data are available from GEO (accession number GSE83493).

RESULTS

Proteomic analysis of polysomes reveals increased recruitment of alternative splicing factors during mitosis

To identify mRNA-binding proteins that are differentially associated with the translation machinery during mitosis, HeLa S3 cells were fully labelled with either light or heavy SILAC amino acids and synchronized to G1 or mitosis using double-thymidine block (4). Intact ribosome-nascent chain complexes were then isolated by ultracentrifugation of cell lysates through sucrose gradients, followed by fractionation with continuous monitoring of rRNA absorption at 254 nm. Polysome-containing fractions were pooled and proteins were precipitated and analyzed by LC-MS/MS (Figure 1A). As previously reported, synchronization of cells to mitosis using double-thymidine block resulted in similar levels of polysomes (Figure 1B) despite attenuation of translation rates (3,4). Major protein components of isolated polysome samples were similar between G1 and mitosis, as evidenced by silver staining of the pooled gradient fractions (Figure 1C). MS analysis of the same gradient fractions showed that ribosomal proteins comprise about 80% of the protein mass in the sample, and are generally invariant between G1 and mitosis (Figure 1D, green) thus driving the high correlation between the two phases (Pearson's r = 0.99). Of the 1,267 unique proteins identified, 45% were previously annotated as RNA binding (8) (Figure 1D, purple and blue). While the majority of those were found to be similarly associated with polysomes in G1 and mitosis, a subset of proteins consisting mostly of alternative splicing factors was enriched on mitotic polysomes (Figure 1D, blue), including members of the serine/arginine-rich (SR) splicing enhancers and heterogeneous nuclear ribonucleoprotein (hnRNP) splicing repressors (for a complete list of proteins identified, see Supplementary Table S2). To narrow down the list to potential candidates that are most significantly enriched on mitotic polysomes, we filtered our dataset for proteins showing a minimum increase of 2 fold as compared to G1 (P-value < 0.01), whose abundance represents a minimum ratio of 1 copy per 50 ribosomes based on mean normalized intensity (iBAQ intensity, mitosis). This resulted in a list of 13 predominantly-nuclear proteins (Figure 1E), including several SR proteins and hnRNPs (SRSF1, SRSF7, SRSF10/FUSIP, HNRNPC, HNRNPG/RBMX, RALY), as well as the splicing regulators Enhancer of rudimentary homolog (ERH) and Transformer-2 protein homolog beta (TRA2B), and members of the splicing-dependent exon-junction complex (EJC) (ACIN1, PNN, DDX39B/BAT1, THOC4/ALYREF, EIF4A3). The increased interaction of these 13 proteins with mitotic polysomes was not associated with statistically-significant differences in their overall cellular abundance (Supplementary Table S3). Interestingly, hnRNP C has been implicated in regulating cap-independent translation of PDGFB (C-sis) during megakaryocyte differentiation, as well as MYC (c-Myc) and CSDE1 (Unr) during cell division (24–26); furthermore, SRSF1 was previously reported to regulate both splicing and translation

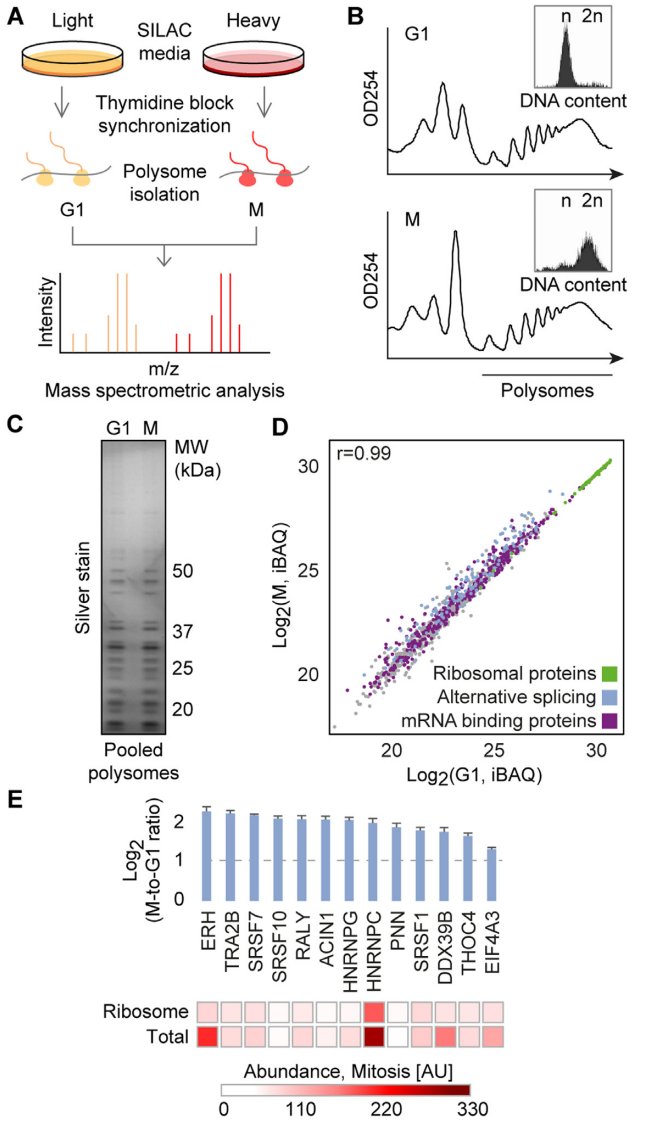

Figure 1. Proteomic screen reveals increased association of alternative splicing factors with polysomes during mitosis. (**A**) Experimental design of proteomic screen. HeLa S3 cells were cultured in either heavy or light isotope labeled (SILAC) amino acids for 10 days, then synchronized to G1 or mitosis (M), respectively, by double-thymidine block. Polysomes from G1 and M cells were isolated by ultracentrifugation through sucrose gradients and analyzed by mass spectrometry (MS). (**B**) Polysome profiles of cells synchronized to G1 (top panel) and M (bottom panels). Insets show DNA content analysis by PI staining and flow cytometry, reflecting a mitotic population of ∼5% and 85% in samples denoted G1 and M, respectively. (**C**) Silver staining of proteins extracted from the combined polysomal fractions of the gradients showing lack of major differences in protein composition of polysomes in G1 and M. (**D**) Scatter plot of iBAQ-normalized MS intensities. In green are ribosomal proteins, which represent ∼80% of protein mass in the polysomal fractions. In purple are mRNA binding proteins according to Gene Ontology Molecular Function (GOMF) annotation and (8). In blue are proteins involved in alternative splicing, many of which are enriched on mitotic polysomes. (**E**) Proteins showing a minimum increase of 2 fold from G1 to mitosis (P-value < 0.01), whose abundance represents a minimum ratio of one copy per 50 ribosomes based on mean normalized intensity (iBAQ intensity, mitosis). Bar plot represents the logarithmic ratio of normalized MS intensities for M over G1; heatmaps reflect the relative abundance of each protein during mitosis in either ribosome-associated ('Ribosome') or total proteome ('Total') samples.

of mRNAs required for normal mitotic progression (27). Thus, the observation that both hnRNP C and SRSF1 are recruited to polysomes during mitosis lends further support to our experimental approach.

Top candidates identified by proteomic analysis are associated with elongating polysomes, but not spliceosomes, during mitosis

The top 13 candidates identified above are nuclear mRNA-binding proteins with known roles in splicing. To confirm these are indeed associated with polysomes and not spliceosomes that may become dispersed throughout the cytoplasm following nuclear envelope breakdown, we synchronized HeLa S3 cells to mitosis and induced translation termination with puromycin, an irreversible inhibitor of nascent chain elongation that leads to polysome disassembly. We reasoned that a brief pulse of puromycin leading to partial disassembly would allow us to detect ribosome runoff and redistribution of ribosomal proteins while keeping indirect stress-related effects to a minimum. A similar redistribution of the protein candidates would then suggest that they are associated with puromycin-sensitive polysomes. Fractionation on a sucrose gradient followed by immunoblotting of gradient fractions showed partial puromycin-induced dissociation of polysomes, as evidenced by a shift of both ribosomal RNA (Figure 2A) and ribosomal protein L26 (RPL26, or uL24 according to the new nomenclature system (28); Figure 2B, top panel) towards the lighter fractions. We then explored the distribution of core spliceosomal components in the same gradients and found they did not co-sediment with ribosomal proteins regardless of puromycin treatment, as evidenced by the non-overlapping distribution of ribosomal protein S10 (RPS10, or eS10) and spliceosomal proteins SmB/B' and SmD (Figure 2B, second panel from the top). Next, we assayed the distribution of 7 of the 13 proteins predicted to be associated with polysomes; 6 of those showed a puromycin-sensitive pattern of co-sedimentation with polysomes (all except for SRSF1, which co-sediments with 40S subunits; Figure 2C). In contrast, hnRNP F, which was not predicted to be recruited to polysomes by our MS screen, did not co-sediment with polysomes (Figure 2C, bottom panel) confirming that polysomal interactions are not characteristic of all mRNA-binding proteins released from the nucleus during mitosis. This puromycin-sensitivity assay therefore indicated that only specific mRNA-binding proteins become associated with mitotic polysomes and may play a role in regulating translation during mitosis.

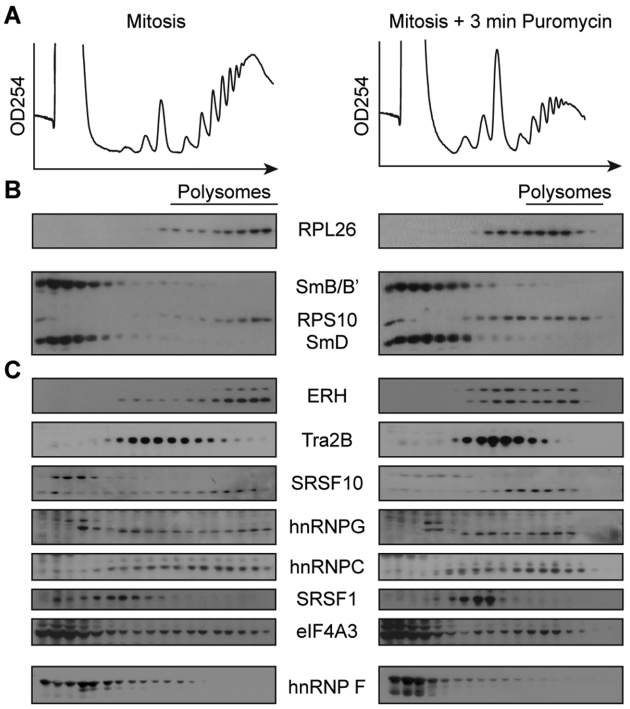

Figure 2. Candidates identified by proteomic analysis are associated with elongating ribosomes, but not splicesomes, during mitosis. (**A–C**) Cells were synchronized to mitosis by double-thymidine block and treated with 1 μM puromycin for 3 min at 37°C to induce partial collapse of polysomes. Control and puromycin-treated mitotic cells were subjected to polysome profiling by ultracentrifugation through a sucrose gradient (A). Proteins extracted from fractions of the gradients were subjected to immunoblot analysis using anti-RPL26 or Y12 anti-Sm antibody, which detects spliceosomal proteins SmB/B' and SmD but also cross reacts with RPS10 (16) (B). Same membranes were reprobed with antibodies against seven of the proteins identified by proteomic analysis as enriched on polysomes during mitosis, and anti-hnRNP F as negative control (C).

Association of hnRNP C with elongating ribosomes increases during mitosis

Most striking of the top candidates in Figure 1E, not only in terms of fold-enrichment but also absolute abundance on mitotic polysomes, was hnRNP C—a ubiquitous and predominantly nuclear protein first identified as a component of the hnRNP core particle, which sorts newly-transcribed mRNAs into various maturation pathways (29). Of the 23 hnRNPs identified in our MS analysis, only hnRNP C and two others (hnRNP G and hnRNP H3) were enriched >2-fold on mitotic polysomes (Figure 3A, bar plot), implying that the association of these proteins with polysomes may be distinct from their role in the core hnRNP particle. While hnRNP C is among the most abundant of this family of proteins, mere abundance is not enough to explain its recruitment to polysomes, as similarly abundant proteins e.g. hnRNP A2B1, hnRNP A1 and hnRNP K showed negligent polysomal association during mitosis (Figure 3A, heatmap). Furthermore, no hnRNP showed a statistically-significant increase in total expression levels from G1 to M (Supplementary Table S3).

To confirm that the occupancy of hnRNP C on polysome increases from G1 to mitosis, we isolated polysomes from cytoplasmic lysates of synchronized cells by ultracentrifugation through a sucrose cushion. While similar amounts of Poly-A binding protein (PABP) co-sedimented with ribosomes in G1 and M, about three times more hnRNP C was found in the ribosomal pellet from mitotic cells (Figure 3B; P-value = 0.0015). Unlike the MS measurements of total protein levels, which were performed on whole cell lysates, these blots were performed using cytoplasmic lysates; therefore, the increase in cytoplasmic levels of hnRNP C during mitosis (Figure 3B) reflects release of the nuclear protein rather than altered expression. Furthermore, fraction-

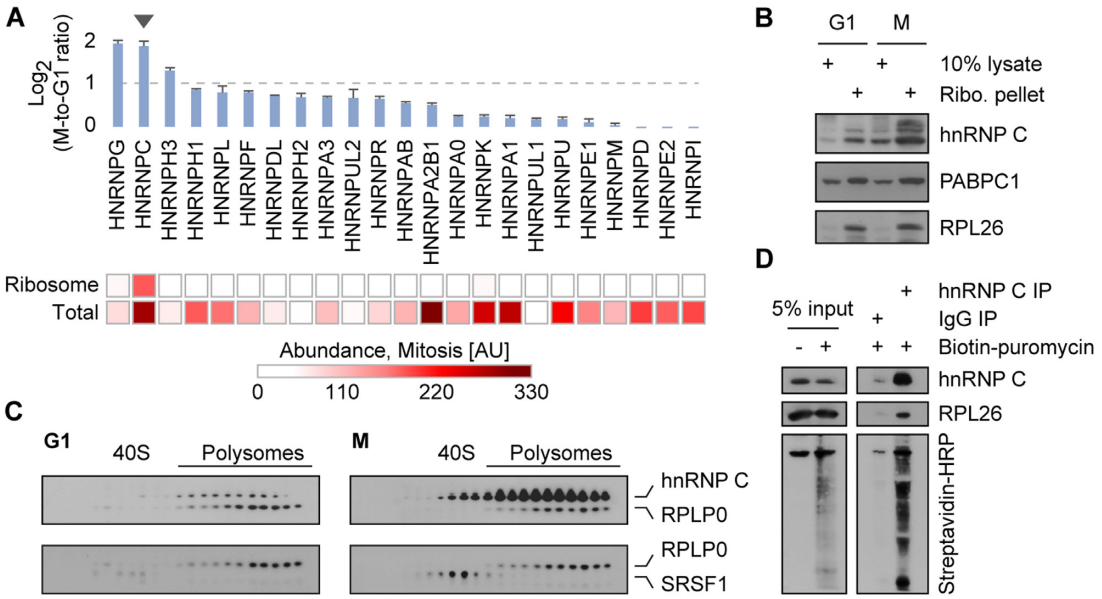

Figure 3. Association of hnRNP C with polysomes increases from G1 to mitosis. (**A**) MS measurements of members of the hnRNP family. Bar plot represents the logarithmic ratio of normalized MS intensities for M over G1; heatmaps reflect the relative abundance of each protein during mitosis in either ribosome-associated ('Ribosome') or total proteome ('Total') samples. (**B**) Polysomes were extracted from G1 and M cytoplasmic lysates by ultracentrifugation through a sucrose cushion, and protein content of the lysates and pellets was monitored by immunoblotting using antibodies to hnRNP C, Poly-A binding protein (PABPC1) and Ribosomal protein L26 (RPL26). (**C**) Polysomes were extracted from G1 and M cells by ultracentrifugation through a sucrose gradient, and protein content of each fraction was monitored by immunoblotting using antibodies to Ribosomal protein P0 (RPLP0) and either hnRNP C (top panel) or SRSF1 (bottom panel). The membrane was simultaneously incubated with either pair of antibodies to allow a more direct comparison of protein amounts. 40S, small ribosomal subunit. (**D**) Polysomes were extracted as in (A) and hnRNP C-bound complexes were immunoprecipitated using antibodies to hnRNP C or IgG as control, followed by incubation with biotin-conjugated puromycin to label nascent polypeptide chains. 5% of polysome pellet and 100% of hnRNP C IP were then subjected to immunoblot analysis using anti-hnRNP C and anti-RPL26, as well as streptavidin-HRP.

ation of cytoplasmic lysates through a sucrose gradient revealed that, during mitosis, more hnRNP C co-sediments with ribosomal protein P0 (RPLP0, or uL10) in a pattern indicative of polysomal association (Figure 3C). In contrast, SRSF1 did not co-sediment with RPLP0 despite showing increased cytoplasmic abundance during mitosis (Figure 3C). Prolonged treatment with puromycin showed that upon near-complete dissociation of polysomes, hnRNP C co-sediments with PABP but not RPL26, confirming its association with polysomes is mediated by binding to mRNA rather than rRNA or ribosomal proteins. (Supplementary Figure S1).

To better characterize the translational status of hnRNP C-containing polysomes during mitosis, we used an immunoprecipitation-based approach to isolate ribosome-mRNA complexes bound to hnRNP C. We first extracted ribosomes from mitotic cells by ultracentrifugation of cytoplasmic lysates through a sucrose cushion, followed by immunoprecipitation of hnRNP C-containing complexes using a monoclonal antibody against the endogenous protein (4F4). Then, isolated ribosomal complexes were incubated with biotinylated puromycin to incorporate a biotin label into nascent polypeptide chains (5), followed by separation of the labeled chains on an SDS-PAGE. Both RPL26 and puromycin-labelled nascent chains were found to co-precipitate with hnRNP C but not with IgG control (Figure 3D), confirming that hnRNP C associates with elongating ribosomes during mitosis.

Finally, we used confocal microscopy to evaluate the spatial redistribution of hnRNP C and ribosomal proteins as cells progress from G1 to mitosis. By staining with antibodies against endogenous RPS6, hnRNP C and hnRNP F as a negative control, we observed that both hnRNP C and F are restricted to the nucleus during interphase, while RPS6 is predominantly cytoplasmic (Figure 4A, C). This is consistent with hnRNP C having a nuclear retention signal, as previously reported (30), which prevents its export to the cytoplasm. After nuclear envelope breakdown, hnRNP C and F are released into the cytoplasm, but while hnRNP F shows a diffuse pattern (Figure 4D), hnRNP C demonstrates a striking ring-like accumulation at the cell membrane (Figure 4B). This pattern of regulated spatial organization was also observed in mitotic U2OS cells (Supplementary Figure S2), and is reminiscent of the subcellular redistribution of hnRNP A1 following osmotic stress and UV exposure, which was shown to be associated with altered translation of anti- and pro-apoptotic mRNAs (31,32). The strong overlap in signal between hnRNP C and RPS6 at the cell periphery (Figure 4A) suggests that hnRNP C, but not hnRNP F, may be associated with a subset of polysomes at this specific subcellular location.

hnRNP C regulates the expression of ribosomal proteins and translation factors

To test the effect of hnRNP C on translation, we generated a conditional knockdown in HeLa S3 cells by stably

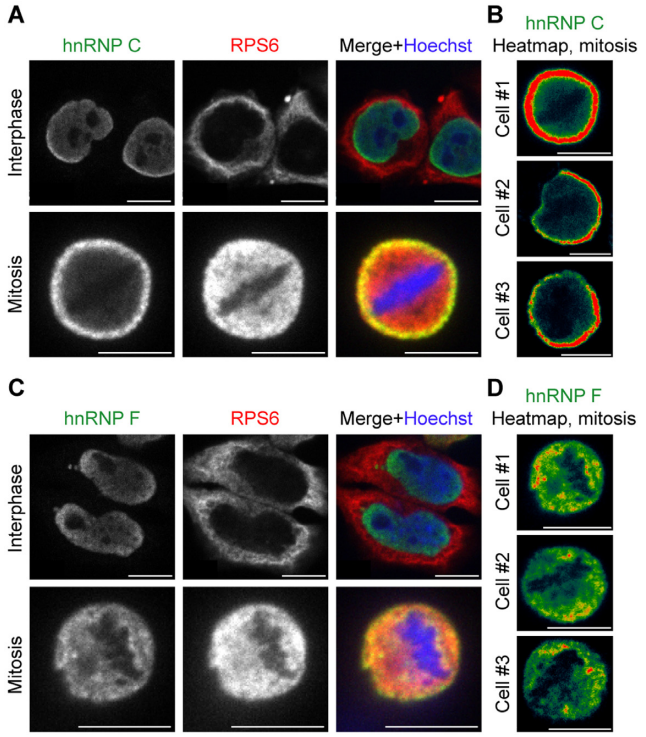

Figure 4. hnRNP C, but not hnRNP F, localizes at the cell periphery during mitosis. (**A** and **B**) Confocal immunofluorescent analysis of non-synchronized HeLa cells stained for DNA (blue), RPS6 (red) and either hnRNP C (**A**) or hnRNP F (**B**) (green). Shown are representative images from a single plane of interphase or mitotic cells. (**C** and **D**) Pseudocolor (heatmap) rendition of a single confocal midplane of the hnRNP C (C) or hnRNP F (D) channels in three representative mitotic cells. Depiction of per-pixel signal intensities ranges from dark blue (low) to red (high). Scale bar, 10 μm.

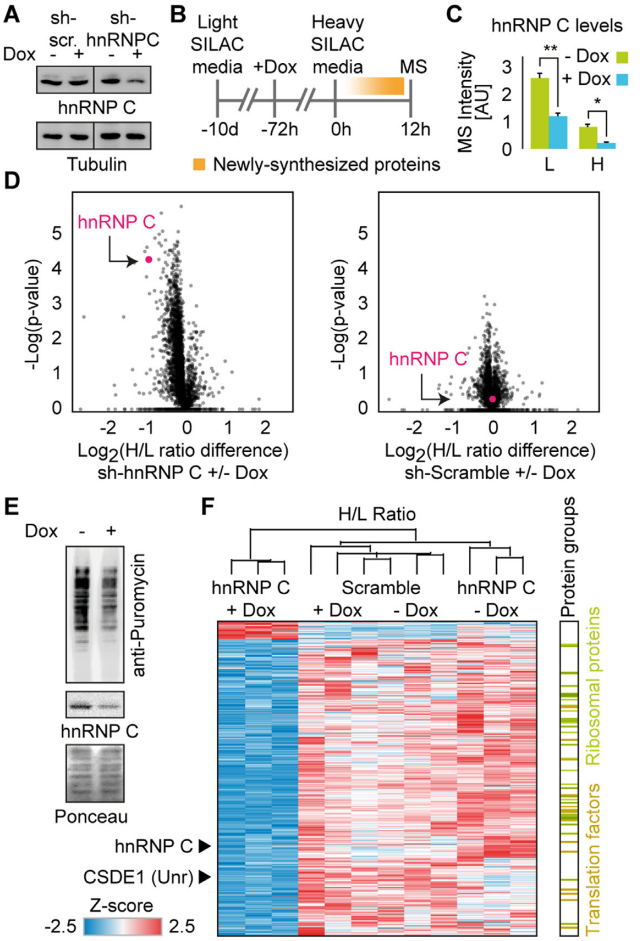

Figure 5. Knockdown of hnRNP C results in reduced global translation rates. (**A**) sh-hnRNP C and sh-Scramble cells were treated with Dox for 72 h to induce hnRNP C knockdown. Knockdown efficiency was confirmed by immunoblotting. (**B**) Experimental design to test the effect of hnRNP C knockdown on protein synthesis. sh-hnRNP C and sh-Scramble cells were labeled with light (L) SILAC media for 10 days to label preexisting proteins and then subjected to Dox treatment for additional 72 h to induce the expression of hnRNP C shRNA or scrambled shRNA, followed by incubation in heavy (H) SILAC media to label newly-synthesized proteins. At 12 h of labeling, cells were harvested and subjected to MS analyses. (**C**) Amounts of preexisting (L) and newly-synthesized (H) hnRNP C levels in Dox-treated and untreated sh-hnRNP C cells, as measured by MS. **P*-value = 0.015, ***P*-value = 0.0073. *P* values were calculated using a two-tailed Student's *t*-test. (**D**) Volcano plots for the ratios of newly-synthesized (H) to preexisting proteins (L) for Dox-treated versus untreated sh-hnRNP C (left) and sh-Scramble (right). (**E**) Puromycin metabolic labeling assay to detect protein synthesis rates upon hnRNP C knockdown in sh-RNPC HeLa cells. (**F**) Heatmap showing hierarchical clustering of proteins with statistically significant differences in synthesis levels for sh-hnRNP C and sh-Scramble (ANOVA, FDR < 0.01). Note the over-representation of ribosomal proteins and translation factors among the cluster of downregulated proteins (blue) upon hnRNP C knockdown (right panel).

expressing doxycycline (Dox)-inducible shRNA against hnRNP C. Previous studies have shown that hnRNP C knockdown or knockout is viable but associated with growth defects, possibly due to delayed cell cycle progression (33,34). Treating sh-hnRNP C cells with Dox for 72 h resulted in a notable reduction of hnRNP C levels, compared to sh-Scramble cells stably expressing Dox-inducible scrambled shRNA as control (Figure 5A), but did not significantly affect cell cycle progression (Supplementary Figure S3). To measure the synthesis rates of different proteins in the proteome, we then performed a pulsed SILAC experiment, in which cells were first cultured for 10 days with light SILAC amino acids (L), then pretreated with Dox for additional 72 h to induce hnRNP C knockdown, followed by incubation in media containing both Dox and heavy SILAC amino acids (H) for additional 12 h to label newly-synthesized proteins (Figure 5B). A labeling duration of 12 h was chosen because shorter pulses do not allow sufficient incorporation of the label into newly-synthesized proteins (5,35). At 12 h, cells were harvested and total protein was processed for MS analysis. This experiment was performed in triplicates for each of four conditions, namely Dox-treated and untreated sh-hnRNP C or sh-Scramble cells, to control for non-specific effects of Dox on protein synthesis. MS analysis detected a reduction of 53% and 73% in preexisting (L) and newly-synthesized (H) hnRNP C protein levels, respectively, in response to Dox treatment (Figure 5C and Supplementary Table S4). Interestingly, the synthesis rates of most proteins were mildly reduced in response to Dox treatment of sh-hnRNP C but not sh-Scramble cells, as demonstrated by the ratios of heavy-to-light labels that represent the ratio between newly-synthesized and preex-

isting proteins (Figure 5D). To confirm that the difference in ratios reflects reduced translation rates in cells depleted of hnRNP C, we labeled newly synthesized proteins by incubating Dox-treated and untreated non-synchronized sh-hnRNP C cells with puromycin for 5 min, followed by immunoblotting of labeled nascent chains on SDS-PAGE using an anti-puromycin antibody (36). Indeed, puromycin labeling confirmed that global translation rates are reduced upon hnRNP C knockdown, suggesting a general impairment of the protein synthesis machinery (Figure 5E).

Of the 3,326 proteins with measured ratios across our MS experiments, 616 showed statistically-significant differences that were specific to the hnRNP C knockdown condition (ANOVA, FDR < 0.01). This group consisted predominantly of proteins whose translation was reduced upon hnRNP C knockdown but not scramble or no-Dox controls (Figure 5F), and included CSDE1 (Unr), whose translation was previously shown to be promoted by hnRNP C during mitosis (26) (for a complete list of proteins identified, see Supplementary Table S4). Analysis of Gene Ontology functions revealed that this group is enriched for annotations related to translation factor activity, ribosomes and the cell cycle (Figure 5F, right panel), supporting a potential role for hnRNP C in the production of translation machinery components (for a complete list of enriched terms, see Supplementary Table S5).

Loss of hnRNP C affects the translation efficiency of mRNAs encoding ribosomal proteins during mitosis

While our pSILAC experiment showed an effect of hnRNP C knockdown on translation, it was performed using non-synchronized cells and thus did not provide the temporal resolution needed to establish a specific connection to mitosis. Furthermore, previous work has shown the importance of alternative splicing to cell cycle progression (37), and the proteomic approach we used could not exclude that the reduced translation rates were due to upstream effects of hnRNP C on splicing or stability of target mRNAs. To address these issues, we next turned to monitor the translatome of synchronized cells using ribosome profiling. First, we evaluated whether Dox induction of hnRNP C knockdown can be combined with cell synchronization using double-thymidine block. Culturing sh-hnRNP C cells in Dox-supplemented media for 72 h followed by double-thymidine block synchronization in the presence of Dox resulted in a reduction of hnRNP C levels with just a minor effect on synchronization, as evidenced by the levels of the mitotic marker Cyclin B1 (Figure 6A) and flow cytometry analysis (54% vs. 58% mitotic cells in thymidine-synchronized Dox-treated and untreated cells, respectively; Supplementary Figure S4). To monitor the abundance and translation rates of specific mRNAs in mitotic cells depleted of hnRNP C, we performed RNA-seq and ribosome profiling (Ribo-seq) on Dox-treated and untreated sh-hnRNP C cells synchronized to mitosis. Using these datasets, we explored the possibility that the effects of hnRNP C depletion on translation were secondary to its role in alternative splicing. Analysis of the RNA-seq data allowed us to measure changes in transcript expression levels and detect alternative splicing events, while combined analysis of the RNA-seq and Ribo-seq datasets enabled us to monitor changes in translation efficiency (TE). Overall, we detected 283 transcripts whose splicing was altered upon hnRNP C depletion. However, these did not show a general change in either mRNA abundance or TE as compared to the entire transcriptome (Supplementary Figure S5), suggesting there is no direct link between the role of hnRNP C in splicing and its role in translation. Nevertheless, a few mRNAs in this subset do confirm that splicing can indirectly affect translation through stabilization or destabilization of transcripts. For example, we found that loss of hnRNP C is associated not only with aberrant splicing of CD55 (Decay-accelerating factor, DAF), as previously reported (38,39), but also with a concordant increase in its total as well as ribosome-protected mRNA levels (31 and 45% increase; respectively; P-value $< 10^{-10}$ in both cases) (Supplementary Figure S6). Our proteomic data further confirmed that the synthesis of CD55 increases by 49% in the absence of hnRNP C (P-value $= 0.04$), suggesting that hnRNP C-mediated splicing may indirectly affect the amount of CD55 translation products through modulation of its mRNA stability. However, for most transcripts aberrant splicing in the absence of hnRNP C was not associated with any effects on mRNA stability or translation efficiency (e.g. UBC [Ubiquitin]; Supplementary Figure S7). Taken together, these results suggest that the role of hnRNP C in splicing may be distinct from its regulatory role in translation during mitosis, and that these may involve different subsets of mRNAs.

We next examined the combined RNA-seq and Ribo-seq dataset for effects of hnRNP C depletion on translation during mitosis. Following up on the results of our proteomic analysis that implicated hnRNP C in the biosynthesis of ribosomal proteins and translation factors, we evaluated whether hnRNP C depletion was associated with changes in transcript levels and ribosome footprints of mRNAs encoding components of the translation machinery. This analysis found that upon hnRNP C depletion, transcripts with translation-related annotations (Gene Ontology Biological Process [GOBP] 'Translation') show reduced ribosome occupancy during mitosis (Figure 6B, left; P-value $= 1.07 \times 10^{-13}$) although their total mRNA levels are slightly increased (Figure 6B, right; P-value $= 1.78 \times 10^{-5}$). Furthermore, while hnRNP C depletion had no effect on the TE of transcripts encoding proteins with known mitotic functions (GOBP 'Mitosis'; P-value $= 0.49$), it resulted in a mild but statistically significant reduction in the TE of mRNAs encoding ribosomal proteins (Gene Ontology Cellular Compartment [GOCC] 'Ribosome' annotation; P-value $= 9.92 \times 10^{-12}$) (Figure 6C). Interestingly, a recent study found that mRNAs encoding for ribosomal proteins are efficiently translated during mitosis (40); to test the hypothesis that hnRNP C facilitates translation of ribosomal protein mRNAs in mitotic cells, we extracted RNA from sucrose gradients of Dox-treated and untreated sh-hnRNP C cells synchronized to mitosis, and performed quantitative real-time PCR (qPCR) on selected transcripts encoding ribosomal and other control proteins. This analysis showed that, while polysomes remain intact upon depletion of hnRNP C from mitotic cells (Figure 6D), mRNAs encoding RPS18, RPL12, RPS9 and RPL34 shift from polysome to sub-polysome fractions (Figure 6E), suggesting their trans-

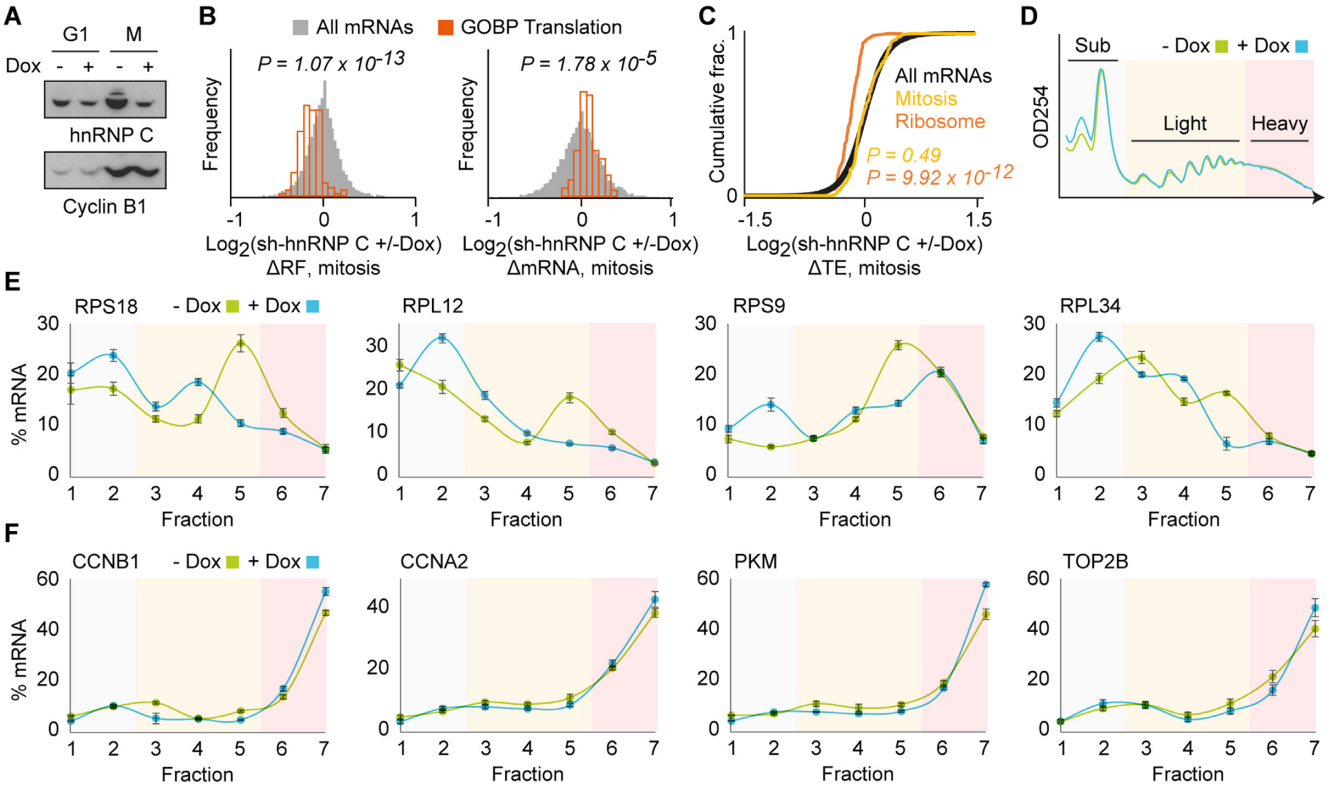

Figure 6. hnRNP C promotes translation of ribosomal proteins during mitosis. (**A**) hnRNP C knockdown was induced for 72 h followed by double-thymidine block synchronization in the presence of Dox. Knockdown efficiency was confirmed by immunoblotting. (**B**) Histograms of the difference in ribosome footprints (ΔRF, left) and total mRNA (ΔmRNA, right) between hnRNP C knockdown (+Dox) and control (–Dox) mitotic sh-hnRNP C cells, showing reduced ribosome association of mRNAs encoding translation-related proteins (GOBP 'Translation' annotation), despite a slight increase in their overall mRNA levels. (**C**) Cumulative distribution of translation efficiency (TE) fold-changes for ribosomal (GOCC 'Ribosome' annotation) and mitotic (GOBP 'Mitosis' annotation) proteins compared to the entire transcript dataset. *P* values for B and C were calculated using a two-tailed Wilcoxon rank-sum test. (**D**) Polysome profiles of mitotic sh-hnRNP C cells with and without Dox. (**E** and **F**) qPCR analysis with primers specific for the indicated ribosomal protein transcripts (**E**) or control transcripts (F), performed on RNA isolated from sucrose gradient fractions as shown in (D). Error bars were calculated from three biological replicates, each subjected to three independent qPCR analyses.

lation is at least partially dependent on hnRNP C. In contrast, no change in polysome association was detected for control transcripts encoding cyclins (CCNB1 and CCNA2), pyruvate kinase (PKM) and DNA topoisomerase 2-beta (TOP2B) (Figure 6F).

DISCUSSION

In this work, we set out to evaluate how the composition of polysome-associated mRNA-binding proteins changes along the cell cycle and identify factors that may play a regulatory role in mitotic translation. Our unbiased proteomic screen found multiple splicing factors to be significantly enriched on mitotic polysomes; of those, we chose hnRNP C for further validation as a candidate regulator of mitotic translation. hnRNP C was a highly attractive test case, as it was previously shown to regulate the translation of c-Myc and Unr mRNAs during mitosis by trans-activating internal ribosome entry sites (IRES) within their 5′ UTRs (25,26). Moreover, we detected very high levels of hnRNP C in polysomal fractions from mitotic cells (Figure 1E), suggesting it may regulate the translation of a large and possibly diverse mRNA population. It was also shown to be phosphorylated during mitosis (41), a modification which could modulate its binding to different subsets of mRNAs. Furthermore, increased hnRNP C nucleocytoplasmic shuttling prior to mitosis was found to be essential for normal cell cycle progression (33).

To first establish that the observed association of hnRNP C with polysomes during mitosis does not simply reflect nuclear envelope breakdown followed by mixing of the nuclear and cytoplasmic pools of proteins, we used a combination of analytical ultracentrifugation, puromycin-sensitivity and nascent chain pulldown assays and confirmed that hnRNP C binds to elongating ribosomal complexes during mitosis, while other highly-abundant nuclear mRNA-binding proteins (e.g. SmB/B', hnRNP F, SRSF1) do not. Furthermore, immunofluorescence analysis suggested that hnRNP C, but not hnRNP F, is associated with a subset of ribosomes that are spatially distributed to the cell periphery and may be membrane bound. Proteomic, biochemical and deep-sequencing analyses revealed that hnRNP C knockdown leads to a global decrease in the synthesis rates of most proteins. This global decrease was not due to aberrant splicing, but was driven at least in part by the transcript-specific effects of hnRNP C depletion on translation of mRNAs encoding ribosomal proteins and translation factors,

as demonstrated by both proteomic and ribosome profiling analyses.

hnRNP C is known to bind around alternatively spliced or cryptic exons where it competes with the core splicing factor U2AF65.6 and protects from aberrant exonization (39). Nevertheless, our data suggest that the role of hnRNP C in splicing is distinct from its role as a translational regulator (Supplementary Figure S5). While hnRNP C-mediated splicing of most transcripts does not seem to affect their abundance or translation rates (e.g. UBC, Supplementary Figure S7), it may in some cases affect mRNA stability and thus promote a secondary increase or decrease in the amounts of translated product (e.g. CD55, Supplementary Figure S6). It has long been known that hnRNP C depletion results in increased exon inclusion and thus translation of a secreted instead of membrane-bound form of CD55 protein (38,39). Increased exon inclusion of CD55 transcript was also observed in our mitotic RNA-seq data, and this was associated with a concordant increase in total as well as ribosome-associated mRNA levels of CD55, while translation efficiency remained unchanged. Furthermore, our proteomic data support a concordant increase in both newly-synthesized and steady-state protein levels of CD55 upon hnRNP C knockdown.

As for a possible mechanism of activity, hnRNP C might promote mRNA translation by displacing inhibitory RNA binding proteins and relieving their translational block. A similar model was suggested for the role of hnRNP C in translation of amyloid precursor protein (APP) mRNA in neuroblastoma cells, where it competes with Fragile X mental retardation protein (FMRP) for binding to the same region of the transcript and prevents translational silencing through recruitment to processing bodies (42). In our cell cycle model, the combined proteomic and ribosome profiling results support a role for hnRNP C in trans-regulation of ribosomal protein mRNAs during mitosis. Furthermore, hnRNP C was previously shown to promote the translation of c-Myc mRNA during mitosis (25); in turn, c-Myc enhances both transcription and translation of ribosomal mRNAs (43,44). As ribosome biogenesis is tightly coupled to cell cycle progression (15,45), it is tempting to speculate that hnRNP C may represent a critical factor that coordinates both processes to guarantee adequate levels of ribosomes and other components of the translation machinery as daughter cells enter G1.

Surprisingly, while global translation rates are reduced following hnRNP C knockdown, as evidenced by metabolic labeling and pulsed SILAC analysis, this is not reflected in polysome profiles (Figure 5D). The stabilization of mitotic polysomes due to reduced translation elongation of some, but not all, mRNAs (3) implies that heavy polysomes are not a reliable readout of active translation under certain conditions. Importantly, this suggests that some mitotic polysomes actively translate specific subclasses of mRNAs while others become translationally stalled and stabilized (5). The current study suggests that hnRNP C may regulate the active translation of specific mRNAs via a yet-undefined mechanism. In contrast to earlier works, reducing the levels of hnRNP C did not have a notable effect on mitotic progression, as evidenced by flow cytometry analysis and expression of mitotic markers (Figure 5A and C, GOBP Mitosis). This could be explained by the relatively mild reduction of hnRNP C protein levels induced by our conditional knockdown (Figures 4A and 5A), as the cumulative effects of hnRNP C depletion on cell viability begin to manifest only after multiple division cycles (data not shown).

In this study, we chose to focus on a cell division model because translation of specific transcripts is known to be selectively up-regulated despite multiple pathways that suppress global translation initiation and elongation during mitosis, and the mechanisms that mediate this effect are largely unknown (3,5–7). The current study sheds new light on the complex regulatory network of mitotic translation through the identification and validation of several proteins that are enriched on mitotic polysomes (HNRNPG, ERH, SRSF10, EIF4A3, TRA2B, SRSF1; Figures 1E and 2C), some of which are already known to affect translation. One such example is the alternative splicing factor SRSF1, which was previously shown to couple splicing and translation of over 1,000 target transcripts and play an important role in mitotic progression (27). Others, such as ERH and TRA2B, have not been implicated in translation as of yet but are thought to play a central role in cell cycle progression by mediating the splicing of the mitotic motor protein CENP-E pre-mRNA (46) and other transcripts implicated in chromosome biology (47). No role has been reported so far for HNRNPG (RBMX) and SRSF10 in splicing control during mitosis or translation regulation in general, but the latter is known to interact with FUS (fused in sarcoma/translocated in liposarcoma), which is mutated in amyotrophic lateral sclerosis (ALS) and was shown to regulate localized translation of mRNAs associated with the tumor suppressor adenomatous polyposis coli (APC) (48). Interestingly, the distribution of SRSF1 in sucrose gradients (Figure 2; also see (49)) is distinctly different from that of other candidate proteins evaluated; it co-sediments only with monosomes and free ribosomal subunits in a puromycin-insensitive pattern, possibly due to its involvement in regulating translation initiation through enhanced phosphorylation of eIF4E-BP1 (49,50). Other candidates selected for validation in this study were found to associate with heavy polysomes, suggesting that they may function through various other mechanisms that may act at the level of translation elongation. Another possible mechanism of action may be mediated by eIF4A3, whose depletion was shown to disrupt the mitotic spindle and dysregulate neural stem cell division (51). Moreover, eIF4A3 is part of the exon junction complex (EJC), which is deposited during splicing and displaced during the first round of translation. The increase in polysome association of spliced mRNA due to EJC deposition previously provided a general link between splicing and translation (52). Furthermore, the involvement of EJC in nonsense-mediated decay (NMD), a translation-coupled mechanism that eliminates mRNAs containing premature translation-termination codons (PTCs) (53), in combination with our current results showing increased association of eIF4A3 with mitotic ribosomes, raises the possibility that NMD is up-regulated during cellular division. Taken together, our results support a possible global link between splicing and translation in which spliced mRNAs are 'imprinted' with a specific set of splicing regulators that govern their localization and translation during mitosis. Others have already

shown that alternative splicing can alter the *cis*-regulatory landscape of mRNAs and affect the polysome association of different mRNA isoforms (54); this is reminiscent of a similar coupling previously proposed between transcription and translation (reviewed in (55)).

In this work, we employed a quantitative proteomic approach followed by functional assays to detect mRNA-binding proteins that associate with polysomes and thus may act as global or transcript-specific regulators of translation. This approach can be used to screen for such factors in many different cellular and animal models suspected to involve regulation at the level of translation, such as tissue development, viral infection and response to drugs.

SUPPLEMENTARY DATA

Supplementary Data are available at NAR Online.

ACKNOWLEDGEMENTS

Author contribution: O.E.S. and R.A. conceived the study. R.A., S.H. and A.S. designed and performed experiments and analyzed data. T.E. and M.E. performed and analyzed the microscopy experiments. R.E. and T.G. analyzed the deep-sequencing and proteomic data, respectively. OES supervised the research. R.A. and O.E.S. prepared the figures and wrote the manuscript and supplementary material.

FUNDING

Israel Science Foundation (ISF) [1036/12 to O.E.S and 1617/12 to T.G.]; Legacy Heritage Bio-Medical Program of the Israel Science Foundation [1629/13 to O.E.S]; Israel Center of Research Excellence program [I-CORE, Gene Regulation in Complex Human Disease Center No. 41/11 to T.G.]. Funding for open access charge: ISF [1036/12 and 1629/13 to O.E.S.].
Conflict of interest statement. None declared.

REFERENCES

1. Pyronnet,S., Dostie,J. and Sonenberg,N. (2001) Suppression of cap-dependent translation in mitosis. *Genes Dev.*, **15**, 2083–2093.
2. Datta,B., Datta,R., Mukherjee,S. and Zhang,Z. (1999) Increased phosphorylation of eukaryotic initiation factor 2alpha at the G2/M boundary in human osteosarcoma cells correlates with deglycosylation of p67 and a decreased rate of protein synthesis. *Exp. Cell Res.*, **250**, 223–2230.
3. Sivan,G., Aviner,R. and Elroy-Stein,O. (2011) Mitotic modulation of translation elongation factor 1 leads to hindered tRNA delivery to ribosomes. *J. Biol. Chem.*, **286**, 27927–27935.
4. Sivan,G., Kedersha,N. and Elroy-Stein,O. (2007) Ribosomal slowdown mediates translational arrest during cellular division. *Mol. Cell. Biol.*, **27**, 6639–6646.
5. Aviner,R., Geiger,T. and Elroy-Stein,O. (2013) Novel proteomic approach (PUNCH-P) reveals cell cycle-specific fluctuations in mRNA translation. *Genes Dev.*, **27**, 1834–1844.
6. Stumpf,C.R., Moreno,M.V., Olshen,A.B., Taylor,B.S. and Ruggero,D. (2013) The translational landscape of the mammalian cell cycle. *Mol. Cell*, **52**, 574–582.
7. Tanenbaum,M.E., Stern-Ginossar,N., Weissman,J.S. and Vale,R.D. (2015) Regulation of mRNA translation during mitosis. *eLife*, **4**, e07957.
8. Baltz,A.G., Munschauer,M., Schwanhausser,B., Vasile,A., Murakawa,Y., Schueler,M., Youngs,N., Penfold-Brown,D., Drew,K., Milek,M. *et al.* (2012) The mRNA-bound proteome and its global occupancy profile on protein-coding transcripts. *Mol. Cell*, **46**, 674–690.
9. Gerstberger,S., Hafner,M. and Tuschl,T. (2014) A census of human RNA-binding proteins. *Nat. Rev. Genet.*, **15**, 829–845.
10. Marchese,D., de Groot,N.S., Lorenzo Gotor,N., Livi,C.M. and Tartaglia,G.G. (2016) Advances in the characterization of RNA-binding proteins. *Wiley Interdiscipl. Rev. RNA*, **7**, 793–810.
11. Rappsilber,J., Mann,M. and Ishihama,Y. (2007) Protocol for micro-purification, enrichment, pre-fractionation and storage of peptides for proteomics using StageTips. *Nat. Protoc.*, **2**, 1896–1906.
12. Cox,J. and Mann,M. (2008) MaxQuant enables high peptide identification rates, individualized p.p.b.-range mass accuracies and proteome-wide protein quantification. *Nat. Biotechnol.*, **26**, 1367–1372.
13. Cox,J., Neuhauser,N., Michalski,A., Scheltema,R.A., Olsen,J.V. and Mann,M. (2011) Andromeda: a peptide search engine integrated into the MaxQuant environment. *J. Proteome Res.*, **10**, 1794–1805.
14. Schwanhausser,B., Busse,D., Li,N., Dittmar,G., Schuchhardt,J., Wolf,J., Chen,W. and Selbach,M. (2011) Global quantification of mammalian gene expression control. *Nature*, **473**, 337–342.
15. Aviner,R., Shenoy,A., Elroy-Stein,O. and Geiger,T. (2015) Uncovering Hidden Layers of Cell Cycle Regulation through Integrative Multi-omic Analysis. *PLoS Genet.*, **11**, e1005554.
16. Hasegawa,H., Uchiumi,T., Sato,T., Ofuchi,Y., Murakami,S., Honda,S., Hirose,S., Ito,S., Nakano,M., Arakawa,M. *et al.* (1999) High frequency of antibody activity against ribosomal protein S10 in anti-Sm sera from patients with systemic lupus erythematosus. *Lupus*, **8**, 439–443.
17. Elis,E., Ehrlich,M., Prizan-Ravid,A., Laham-Karam,N. and Bacharach,E. (2012) p12 tethers the murine leukemia virus pre-integration complex to mitotic chromosomes. *PLoS Pathogens*, **8**, e1003103.
18. Ingolia,N.T., Brar,G.A., Rouskin,S., McGeachy,A.M. and Weissman,J.S. (2012) The ribosome profiling strategy for monitoring translation in vivo by deep sequencing of ribosome-protected mRNA fragments. *Nat. Protoc.*, **7**, 1534–1550.
19. Langmead,B., Trapnell,C., Pop,M. and Salzberg,S.L. (2009) Ultrafast and memory-efficient alignment of short DNA sequences to the human genome. *Genome Biol.*, **10**, R25.
20. Ingolia,N.T., Ghaemmaghami,S., Newman,J.R. and Weissman,J.S. (2009) Genome-wide analysis in vivo of translation with nucleotide resolution using ribosome profiling. *Science*, **324**, 218–223.
21. Hansen,K.D., Irizarry,R.A. and Wu,Z. (2012) Removing technical variability in RNA-seq data using conditional quantile normalization. *Biostatistics*, **13**, 204–216.
22. Kim,D., Pertea,G., Trapnell,C., Pimentel,H., Kelley,R. and Salzberg,S.L. (2013) TopHat2: accurate alignment of transcriptomes in the presence of insertions, deletions and gene fusions. *Genome Biol.*, **14**, R36.
23. Anders,S., Reyes,A. and Huber,W. (2012) Detecting differential usage of exons from RNA-seq data. *Genome Res.*, **22**, 2008–2017.
24. Sella,O., Gerlitz,G., Le,S.Y. and Elroy-Stein,O. (1999) Differentiation-induced internal translation of c-sis mRNA: analysis of the cis elements and their differentiation-linked binding to the hnRNP C protein. *Mol. Cell. Biol.*, **19**, 5429–5440.
25. Kim,J.H., Paek,K.Y., Choi,K., Kim,T.D., Hahm,B., Kim,K.T. and Jang,S.K. (2003) Heterogeneous nuclear ribonucleoprotein C modulates translation of c-myc mRNA in a cell cycle phase-dependent manner. *Mol. Cell. Biol.*, **23**, 708–720.
26. Schepens,B., Tinton,S.A., Bruynooghe,Y., Parthoens,E., Haegman,M., Beyaert,R. and Cornelis,S. (2007) A role for hnRNP C1/C2 and Unr in internal initiation of translation during mitosis. *EMBO J.*, **26**, 158–169.
27. Maslon,M.M., Heras,S.R., Bellora,N., Eyras,E. and Caceres,J.F. (2014) The translational landscape of the splicing factor SRSF1 and its role in mitosis. *eLife*, e02028.
28. Ban,N., Beckmann,R., Cate,J.H., Dinman,J.D., Dragon,F., Ellis,S.R., Lafontaine,D.L., Lindahl,L., Liljas,A., Lipton,J.M. *et al.* (2014) A new system for naming ribosomal proteins. *Curr. Opin. Struct. Biol.*, **24**, 165–169.
29. Beyer,A.L., Christensen,M.E., Walker,B.W. and LeStourgeon,W.M. (1977) Identification and characterization of the packaging proteins of core 40S hnRNP particles. *Cell*, **11**, 127–138.

30. Nakielny,S. and Dreyfuss,G. (1996) The hnRNP C proteins contain a nuclear retention sequence that can override nuclear export signals. *J. Cell Biol.*, **134**, 1365–1373.
31. Cammas,A., Pileur,F., Bonnal,S., Lewis,S.M., Leveque,N., Holcik,M. and Vagner,S. (2007) Cytoplasmic relocalization of heterogeneous nuclear ribonucleoprotein A1 controls translation initiation of specific mRNAs. *Mol. Biol. Cell*, **18**, 5048–5059.
32. Lewis,S.M., Veyrier,A., Hosszu Ungureanu,N., Bonnal,S., Vagner,S. and Holcik,M. (2007) Subcellular relocalization of a trans-acting factor regulates XIAP IRES-dependent translation. *Mol. Biol. Cell*, **18**, 1302–1311.
33. Yang,F., Yi,F., Han,X., Du,Q. and Liang,Z. (2013) MALAT-1 interacts with hnRNP C in cell cycle regulation. *FEBS Lett.*, **587**, 3175–3181.
34. Williamson,D.J., Banik-Maiti,S., DeGregori,J. and Ruley,H.E. (2000) hnRNP C is required for postimplantation mouse development but Is dispensable for cell viability. *Mol. Cell. Biol.*, **20**, 4094–4105.
35. Schwanhausser,B., Gossen,M., Dittmar,G. and Selbach,M. (2009) Global analysis of cellular protein translation by pulsed SILAC. *Proteomics*, **9**, 205–209.
36. Schmidt,E.K., Clavarino,G., Ceppi,M. and Pierre,P. (2009) SUnSET, a nonradioactive method to monitor protein synthesis. *Nat. Methods*, **6**, 275–277.
37. Dominguez,D., Tsai,Y.-H., Weatheritt,R., Wang,Y., Blencowe,B.J. and Wang,Z. (2016) An extensive program of periodic alternative splicing linked to cell cycle progression. *eLife*, **5**, e10288.
38. Caras,I.W., Davitz,M.A., Rhee,L., Weddell,G., Martin,D.W. Jr and Nussenzweig,V. (1987) Cloning of decay-accelerating factor suggests novel use of splicing to generate two proteins. *Nature*, **325**, 545–549.
39. Zarnack,K., Konig,J., Tajnik,M., Martincorena,I., Eustermann,S., Stevant,I., Reyes,A., Anders,S., Luscombe,N.M. and Ule,J. (2013) Direct competition between hnRNP C and U2AF65 protects the transcriptome from the exonization of Alu elements. *Cell*, **152**, 453–466.
40. Park,J.E., Yi,H., Kim,Y., Chang,H. and Kim,V.N. (2016) Regulation of Poly(A) tail and translation during the somatic cell cycle. *Mol. Cell*, **62**, 462–471.
41. Pinol-Roma,S. and Dreyfuss,G. (1993) Cell cycle-regulated phosphorylation of the pre-mRNA-binding (heterogeneous nuclear ribonucleoprotein) C proteins. *Mol. Cell. Biol.*, **13**, 5762–5770.
42. Lee,E.K., Kim,H.H., Kuwano,Y., Abdelmohsen,K., Srikantan,S., Subaran,S.S., Gleichmann,M., Mughal,M.R., Martindale,J.L., Yang,X. *et al.* (2010) hnRNP C promotes APP translation by competing with FMRP for APP mRNA recruitment to P bodies. *Nat. Struct. Mol. Biol.*, **17**, 732–739.
43. Cole,M.D. and Cowling,V.H. (2008) Transcription-independent functions of MYC: regulation of translation and DNA replication. *Nat. Rev. Mol. Cell Biol.*, **9**, 810–815.
44. Elkon,R., Loayza-Puch,F., Korkmaz,G., Lopes,R., van Breugel,P.C., Bleijerveld,O.B., Altelaar,A.F., Wolf,E., Lorenzin,F., Eilers,M. *et al.* (2015) Myc coordinates transcription and translation to enhance transformation and suppress invasiveness. *EMBO Rep.*, **16**, 1723–1736.
45. Dez,C. and Tollervey,D. (2004) Ribosome synthesis meets the cell cycle. *Curr. Opin. Microbiol.*, **7**, 631–637.
46. Weng,M.T., Lee,J.H., Wei,S.C., Li,Q., Shahamatdar,S., Hsu,D., Schetter,A.J., Swatkoski,S., Mannan,P., Garfield,S. *et al.* (2012) Evolutionarily conserved protein ERH controls CENP-E mRNA splicing and is required for the survival of KRAS mutant cancer cells. *Proc. Natl. Acad. Sci. U.S.A.*, **109**, E3659–E3667.
47. Best,A., James,K., Dalgliesh,C., Hong,E., Kheirolahi-Kouhestani,M., Curk,T., Xu,Y., Danilenko,M., Hussain,R., Keavney,B. *et al.* (2014) Human Tra2 proteins jointly control a CHEK1 splicing switch among alternative and constitutive target exons. *Nat. Commun.*, **5**, 4760.
48. Yasuda,K., Zhang,H., Loiselle,D., Haystead,T., Macara,I.G. and Mili,S. (2013) The RNA-binding protein Fus directs translation of localized mRNAs in APC-RNP granules. *J. Cell Biol.*, **203**, 737–746.
49. Sanford,J.R., Gray,N.K., Beckmann,K. and Caceres,J.F. (2004) A novel role for shuttling SR proteins in mRNA translation. *Genes Dev.*, **18**, 755–768.
50. Michlewski,G., Sanford,J.R. and Caceres,J.F. (2008) The splicing factor SF2/ASF regulates translation initiation by enhancing phosphorylation of 4E-BP1. *Mol. Cell*, **30**, 179–189.
51. Silver,D.L., Watkins-Chow,D.E., Schreck,K.C., Pierfelice,T.J., Larson,D.M., Burnetti,A.J., Liaw,H.J., Myung,K., Walsh,C.A., Gaiano,N. *et al.* (2010) The exon junction complex component Magoh controls brain size by regulating neural stem cell division. *Nat. Neurosci.*, **13**, 551–558.
52. Nott,A., Le Hir,H. and Moore,M.J. (2004) Splicing enhances translation in mammalian cells: an additional function of the exon junction complex. *Genes Dev.*, **18**, 210–222.
53. Shibuya,T., Tange,T.O., Sonenberg,N. and Moore,M.J. (2004) eIF4AIII binds spliced mRNA in the exon junction complex and is essential for nonsense-mediated decay. *Nat. Struct. Mol. Biol.*, **11**, 346–351.
54. Sterne-Weiler,T., Martinez-Nunez,R.T., Howard,J.M., Cvitovik,I., Katzman,S., Tariq,M.A., Pourmand,N. and Sanford,J.R. (2013) Frac-seq reveals isoform-specific recruitment to polyribosomes. *Genome Res.*, **23**, 1615–1623.
55. Dahan,N. and Choder,M. (2013) The eukaryotic transcriptional machinery regulates mRNA translation and decay in the cytoplasm. *Biochim. Biophys. Acta*, **1829**, 169–173.